Electric Power Systems Research 213 (2022) 108774

Contents lists available at ScienceDirect

Electric Power Systems Research

journal homepage: www.elsevier.com/locate/epsr

Two novel current-based methods for locating earth faults in unearthed ring operating MV networks

Tesfaye Amare Zerihun [a,*], Thomas Treider [b], Henning Taxt [a], Lars B. Nordevall [c], Thomas S. Haugan [b]

[a] SINTEF Energy Research, Trondheim, Norway
[b] Norwegian University of Science and Technology - NTNU, Trondheim, Norway
[c] Elvia AS, Oslo, Norway

ARTICLE INFO

Keywords:
Earth fault location
Closed-ring MV network
Distribution network
Impedance method
Negative sequence currents
Zero sequence currents

ABSTRACT

Automated fault location plays a key role in improving the reliability of modern power grids—it helps to reduce the power outage time and the number of affected customers. Earth faults in isolated systems are among the fault types that are difficult to detect and locate with a reasonable accuracy, and there has therefore not been a well-established method for detecting and locating such faults in isolated systems. This paper presents two novel current-based methods for locating earth faults in unearthed closed-ring MV networks. The methods are based on the utilisation of sequence components of standard current and voltage measurement at a primary substation and they do not require new devices or measurements in the field. Both methods are tested with a simulation of a network based on data provided by a Norwegian network operator and their prediction performances were investigated considering different scenarios on fault resistance, load asymmetry and measurement errors. Both methods performed well and showed good accuracy. The simulation results are promising and strengthens the prospect of further testing of the methods in real networks and adoption of the methods for a real-world implementation.

1. Introduction

In modern power systems, self-healing and automation of the grid is increasingly applied to distribution grid with the objective of performing automated fault location, isolation and service restoration. These new applications aim to significantly improve the reliability of the grid as less time will be needed to locate and resolve the faults in the grid.

Fault indication and location are key functionalities in the self-healing and automation of the grid. There are many well established methods for locating most short circuit faults (symmetrical or unsymmetrical faults). However, among these fault types, there has not been a commonly accepted, reliable and efficient method for single phase to earth fault location in ungrounded or compensated networks. Locating single phase earth faults is crucial as it is the most common fault type in the distribution network, representing 50 to 90 % of faults in Nordic countries [1].

1.1. Related work

Several fault location methods for single phase earth faults have been proposed and studied. The methods often consider a radial operation of the grid and they can be broadly divided into centralised and decentralised methods. Centralised methods are mainly based on measurements at a primary substations while distributed approaches use measurements along feeders and a communication infrastructure for collection, coordination and management of these measurements.

Some of the most commonly used centralised approaches are the impedance based methods which are based on measuring the apparent impedance seen from either end of a feeder when a fault occurs. Some works such as [2–6] presented an impedance based fault location methods for distribution grids. The works in [5,6] presented an impedance method for ungrounded distribution networks utilising current and voltage measurements at a primary substation. Where as, the method in [5], in addition to the voltage and current measurements of MV primary substations, considered dynamic load models to achieve higher accuracy. The work in [7] presented earth fault location methods that

* Corresponding author.
E-mail addresses: tesfaye.zerihun@sintef.no (T.A. Zerihun), thomas.treider@ntnu.no (T. Treider), henning.taxt@sintef.no (H. Taxt), lars.nordevall@elvia.no (L.B. Nordevall), thomas.haugan@ntnu.no (T.S. Haugan).

https://doi.org/10.1016/j.epsr.2022.108774
Received 27 January 2022; Received in revised form 18 July 2022; Accepted 29 August 2022
Available online 15 September 2022

mainly utilise zero sequence voltage and current measurements on feeders rearranged to ring structure after the occurrence of a fault. It then calculates the distance to the earth fault from the phase to earth admittance and distribution of the components of the zero sequence current. The method apply, however, to radially operated networks. The main challenge with the impedance based approaches is that the fault current in isolated and compensated networks is often very small to allow a satisfactory fault location accuracy.

Another method is the travelling-wave-based method such as in [8–11] which, theoretically, can give accurate fault location. In this method, by measuring the transient voltage and current waves and their reflection and arrival times at either end of the line, the distance to the fault point can be determined. However, due to the availability of numerous branches and laterals in distribution network, the reflection captured at the substation (beginning of the feeder) may come from other sources in the network (noises and disturbances) and not necessarily only from the fault point [12]. Travelling wave based methods are often complex and incur high implementation cost as they often require high sampling rate and sophisticated measurement equipment. This makes it challenging to apply these methods in real distribution networks.

Recently, there has been also the use of artificial intelligence based methods such as [13–19] which use historical data and develop learning algorithms that can determine fault locations. The work in [18] presented a fault location method for unearthed distribution network using Support Vector Machine (SVM) and wavelet technique, however the method assumes a radial operation and requires closing a switch to form a ring after the occurrence of a fault. Other works such as in [17,20] presented a hybrid method combining Discrete Wavelet Transform (DWT) and artificial neural network (ANN) which only use line currents available from substations. Although these type of methods attracted some attention for some time as they often give fairly accurate performance in simulation studies, the research into this direction seems to be declining, and it is difficult to find evidence of real-life implementations [12].

Decentralised fault location methods are realised by the recent modernisation and automation of the grid with the introduction of intelligent electronic devices (IEDs), smart meters, fault passage indicators (FPI), etc. equipping secondary substations with monitoring and communication capability. The utilisation of these components with a communication infrastructure enabled the distributed fault location. The fault location is carried out either locally by the IEDs or by higher level controllers receiving measurements from the IEDs/ICT devices.

Distributed fault location methods in [21,22] used the measurements from smart meters, though it only works for faults with low fault resistance. Fault passage indicators, supported by advanced sensor and communication technology are used for locating earth faults in [23,24]. A list of FPIs that has been used in real implementations and field tests are presented in [25]. The major drawbacks in using FPI based methods is the dependence on the communication infrastructure and the fact that they are only capable of identifying the faulted section between two FPIs.

Some works such as [26,27] used state estimation based methods where sufficient data is provided to the fault location using recorded data from a set of measurement points such as AMI, SCADA, or PMUs that have been used in distribution grids recently. Other works in [28–31] presented methods to locate earth faults which are solely based on low voltage measurements from secondary substations of the distribution grid. A similar approach called 'Vdip' is presented in [32], but in addition to the voltage monitors at LV side of the distribution grid, the method uses current measurement at the primary MV substation.

Other works such as [33,34] presented decentralised methods that are based solely on current measurements. These methods specifically look into the changes in symmetrical components of currents during fault, assuming that the negative sequence current from the feeding substation up to the fault location is relatively higher compared to the negative sequence current after the fault point.

Recent works such as [35–38] presented decentralised methods to locate faults in meshed distribution networks with distributed energy resources (DERs) using information provided by distributed controllers, Intelligent Electronic Devices (IEDs) and IoT devices such as Directional Fault Passage Indicators (DFPI). In [39], an earth fault location method utilising synchronous measurement from PMUs is proposed for an active distribution grid with DERs. The authors in [37,38], presented a multi agent system based fault location methods for distribution systems in the presence of DERs.

Overall, the distributed fault location methods using sensors, IEDs, FPIs, and IoT devices are becoming increasingly common and they are especially promising for next generation distribution networks with ring or meshed operation and high penetration of DERs. However, compared with other approaches such as the impedance based method, their implementation is often costly.

1.2. Aim and contribution

A reliable and efficient fault location method has to be simple, accurate, cost effective, and shall be applicable in different types of network topologies and configurations. Unlike most short circuit faults which are relatively easy to detect and locate, locating earth faults in unearthed systems is challenging. The various fault location methods presented above had their own strengths and drawbacks. The impedance based methods being the most simple and cost effective but highly dependant on estimation of the system parameters while the distributed method with IEDs and FPIs utilise simple measurements along feeders but with a relatively complex implementation requiring field devices and advanced communication capabilities.

This paper aims to propose a simple and cost effective earth fault location method for isolated systems utilising the readily available measurements at MV primary substations. Considering the architectural changes in a futuristic distribution networks, the method exploits the possibilities arising from a ring operation of MV networks. Closed ring operation is seldom used in medium voltage networks in Norway so far. Historically the network is built as pure radials or as open ring network. Radials and open ring network are easy to monitor and the protective scheme is simple and straight forward. However, to improve the overall reliability in the network, ring networks are getting more and more common. Closed ring operation adds some complexity and may increase vulnerability, but there are also benefits like lower losses and possibly improved fault localisation. The paper presents two methods which are mainly based on sequence components of current measurements and neutral voltage measurements at a substation. Overall, the aim is to develop a method that can:

- locate earth faults with error margin of a few hundred meters.
- deal with different load situations (balanced/unbalanced)
- deal with various fault resistances
- be less costly and easy to implement (with simple logic using current and neutral voltage measurements at a substation)

This paper is limited to fault location of single phase to ground faults considering unearthed MV distribution networks only.

1.3. Organisation of the paper

The paper is organised as follows. Section 2 gives a brief theoretical background on the methods used for locating single phase to ground faults using sequence components. Section 3 presents the proposed methods. In Section 4, a brief description of the system considered for illustration of the performance of the methods is presented. Section 5 presents and discusses the results obtained from the case study investigation. Lastly, conclusive remarks and future works are summarised in Section 6.

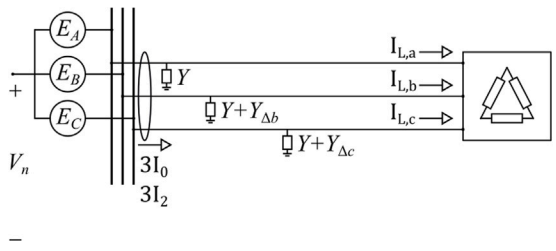

Fig. 1. Healthy feeder.

2. Theory

2.1. Sequence currents in a ring topology

2.1.1. Healthy state

The equations describing the flow of currents on a single feeder is used as the basis for developing a similar set of equations describing the currents on two ring-connected feeders. Consider the feeder in Fig. 1, with phase-ground admittances Y, $Y + Y_{\Delta b}$ and $Y + Y_{\Delta c}$ in phases a, b and c, respectively. The feeder supplies a load with load currents $\vec{I}_{L,a}$, $\vec{I}_{L,b}$ and $\vec{I}_{L,c}$. The phase currents flowing onto the feeder can be derived from Fig. 1 and are given by (1).

$$\begin{aligned}\vec{I}_a &= (\vec{V}_n + \vec{E}_a)Y + \vec{I}_{L,a}\\ \vec{I}_b &= (\vec{V}_n + \vec{E}_b)(Y + Y_{\Delta b}) + \vec{I}_{L,b}\\ \vec{I}_c &= (\vec{V}_n + \vec{E}_c)(Y + Y_{\Delta c}) + \vec{I}_{L,c}\end{aligned} \tag{1}$$

Transforming the phase currents into symmetrical components [40], the zero and negative sequence currents on the feeder are given by (2),

$$\begin{aligned}3\vec{I}_0 &= \vec{V}_n\bar{Y} + \vec{E}_a\hat{Y}\\ 3\vec{I}_2 &= \vec{V}_n\hat{Y} + \vec{E}_a\tilde{Y} + \vec{I}_L\end{aligned} \tag{2}$$

where

$$\begin{aligned}\bar{Y} &= 3Y + Y_{\Delta b} + Y_{\Delta c}\\ \hat{Y} &= h^2Y_{\Delta b} + hY_{\Delta c}\\ \tilde{Y} &= hY_{\Delta b} + h^2Y_{\Delta c}\\ \vec{I}_L &= \vec{I}_{L,a} + h^2\vec{I}_{L,b} + h\vec{I}_{L,c}\end{aligned}$$

have been introduced for more compact notation. The voltage $\vec{E}_a$ is the phase-neutral voltage at the transformer terminal of phase a, $\vec{V}_n$ is the neutral-ground voltage, and $h = e^{j120°}$.

Next, consider instead two feeders, feeders A and B. The phase-ground admittances of feeder A are Y_A, $Y_A + Y_{\Delta b,A}$ and $Y_A + Y_{\Delta c,A}$ as illustrated in Fig. 2. Similarly for feeder B, the phase-ground admittances of the three phases are Y_B, $Y_B + Y_{\Delta b,B}$ and $Y_B + Y_{\Delta c,B}$. If the two feeders are radially operated, the zero and negative sequence currents on each feeder can be described by inserting the admittances and load currents of each feeder into (2). If the two feeders are connected to form a ring, however, the sequence currents measured on the terminals of the two feeders are not straight forward to compute. To overcome this problem, the two ring-connected feeders are treated as a single, equivalent feeder by defining $Y = Y_A + Y_B$, $Y_{\Delta b} = Y_{\Delta b,A} + Y_{\Delta b,B}$ and $Y_{\Delta c} = Y_{\Delta c,A} + Y_{\Delta c,B}$ to maintain the notation used in (1) and (2), and the sum of sequence currents on the two feeders are obtained by (2), here re-written as (3).

$$\begin{aligned}3\vec{I}_{0,A} + 3\vec{I}_{0,B} &= \vec{V}_n\bar{Y} + \vec{E}_a\hat{Y}\\ 3\vec{I}_{2,A} + 3\vec{I}_{2,B} &= \vec{V}_n\hat{Y} + \vec{E}_a\tilde{Y} + \vec{I}_L\end{aligned} \tag{3}$$

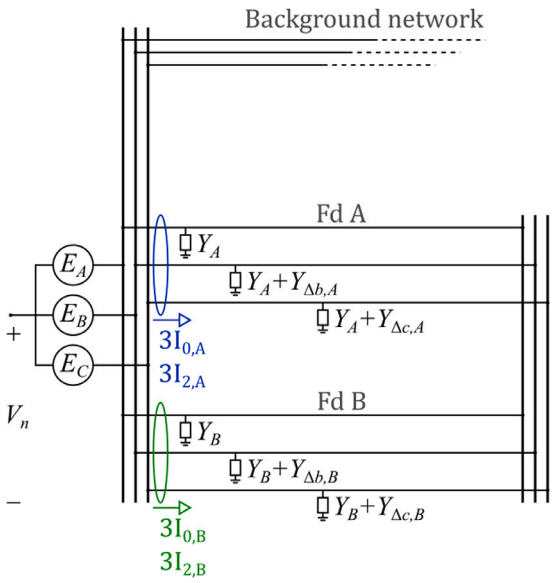

Fig. 2. Ring operating MV distribution network.

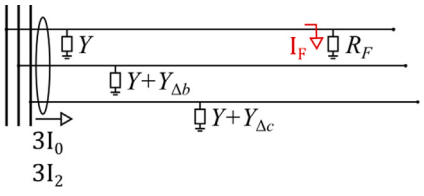

Fig. 3. Earth fault in phase a on a single feeder.

The approach suggested in this paper is to express the sequence currents measured on feeder A and B when connected in a ring as fractions of the sum of sequence currents flowing onto the ring, as described by (4).

$$\begin{aligned}3\vec{I}_{0,A} &= \vec{V}_n\bar{Y}\cdot m_A + \vec{E}_a\hat{Y}\cdot n_A + \vec{I}_{0,ring}\\ 3\vec{I}_{0,B} &= \vec{V}_n\bar{Y}\cdot m_B + \vec{E}_a\hat{Y}\cdot n_B - \vec{I}_{0,ring}\\ 3\vec{I}_{2,A} &= \vec{V}_n\hat{Y}\cdot q_A + \vec{E}_a\tilde{Y}\cdot s_A + \vec{I}_L\cdot t_A + \vec{I}_{2,ring}\\ 3\vec{I}_{2,B} &= \vec{V}_n\hat{Y}\cdot q_B + \vec{E}_a\tilde{Y}\cdot s_B + \vec{I}_L\cdot t_B - \vec{I}_{2,ring}\end{aligned} \tag{4}$$

In (4), all the factors m_A, m_B, n_A, ... $\in [0, 1]$, and $m_A + m_B = n_A + n_B = q_A + q_B = s_A + s_B = t_A + t_B = 1$. These factors are used to describe the general case where each component in the sequence currents may be distributed differently among the two feeders, as will be the case when the feeders' admittances and impedances are not evenly distributed around the ring. The currents $\vec{I}_{0,ring}$ and $\vec{I}_{2,ring}$ are included to account for any circulating sequence currents which may arise from asymmetry in the network [41,42]. These currents will be opposite in polarity on the two feeders, and hence they are not observed when considering the sum of currents on the two feeders.

2.1.2. Sequence currents during fault

A ground fault is assumed to occur in phase a somewhere on the feeder in Fig. 3. Eq. (2) is modified to account for the fault current, and (5) is obtained.

$$\begin{aligned}3\vec{I}_0 &= \vec{V}_n\bar{Y} + \vec{E}_a\hat{Y} + \vec{I}_F\\ 3\vec{I}_2 &= \vec{V}_n\hat{Y} + \vec{E}_a\tilde{Y} + \vec{I}_L + \vec{I}_F\end{aligned} \tag{5}$$

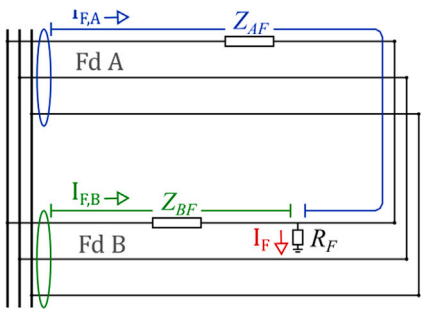

Fig. 4. The impedances Z_{AF} and Z_{BF}.

Using the same approach to describe the currents measured on each feeder in the ring as previously, (4) is rewritten as (6).

$$\begin{aligned} 3\vec{I}_{0,A} &= \vec{V}_n\bar{Y}\cdot m_A + \vec{E}_a\hat{Y}\cdot n_A + \vec{I}_{0,ring} + \vec{I}_{F,A} \\ 3\vec{I}_{0,B} &= \vec{V}_n\bar{Y}\cdot m_B + \vec{E}_a\hat{Y}\cdot n_B - \vec{I}_{0,ring} + \vec{I}_{F,B} \\ 3\vec{I}_{2,A} &= \vec{V}_n\hat{Y}\cdot q_A + \vec{E}_a\tilde{Y}\cdot s_A + \vec{I}_L\cdot t_A + \vec{I}_{2,ring} + \vec{I}_{F,A} \\ 3\vec{I}_{2,B} &= \vec{V}_n\hat{Y}\cdot q_B + \vec{E}_a\tilde{Y}\cdot s_B + \vec{I}_L\cdot t_B - \vec{I}_{2,ring} + \vec{I}_{F,B} \end{aligned} \tag{6}$$

The currents $\vec{I}_{F,A}$ and $\vec{I}_{F,B}$ are the fault current components measured on feeder A and B, respectively.

3. Proposed method

3.1. Estimating the impedance ratio

The per phase series impedances measured along feeders A and B to the fault point are labelled Z_{AF} and Z_{BF}, respectively, as illustrated in Fig. 4. Current division suggests that the ratio of these impedance are the inverse of the ratio of the fault current components $\vec{I}_{F,A}$ and $\vec{I}_{F,B}$, as expressed in (7).

$$\frac{Z_{BF}}{Z_{AF}} = \frac{\vec{I}_{F,A}}{\vec{I}_{F,B}} \tag{7}$$

If the components $\vec{I}_{F,A}$ and $\vec{I}_{F,B}$ can be obtained from measurements, and the impedances of the two lines are known in advance, the distance to fault can easily be estimated. To obtain $\vec{I}_{F,A}$ and $\vec{I}_{F,B}$, the change in zero and negative sequence currents before and after fault inception are utilised as described by (8).

$$\begin{aligned} \Delta 3\vec{I}_{0,A} &= \Delta\vec{V}_n\bar{Y}\cdot m_A + \vec{I}_{F,A} \\ \Delta 3\vec{I}_{0,B} &= \Delta\vec{V}_n\bar{Y}\cdot m_B + \vec{I}_{F,B} \\ \Delta 3\vec{I}_{2,A} &= \Delta\vec{V}_n\hat{Y}\cdot q_A + \vec{I}_{F,A} \\ \Delta 3\vec{I}_{2,B} &= \Delta\vec{V}_n\hat{Y}\cdot q_B + \vec{I}_{F,B} \end{aligned} \tag{8}$$

The Δ-notation introduced in (8) is used to described the change in a current or voltage phasor compared to its value at some pre-fault time t_{pre}. The value of this change at any time t is then $\Delta\vec{I}(t) = \vec{I}(t) - \vec{I}(t_{pre})$.

From (8) the ratio of the fault current components can be found by using either of the two sequence currents. In terms of change in zero sequence current and change in neutral voltage, this ratio is given by (9).

$$\frac{\vec{I}_{F,A}}{\vec{I}_{F,B}} = \frac{\Delta 3\vec{I}_{0,A} - \Delta\vec{V}_n\bar{Y}\cdot m_A}{\Delta 3\vec{I}_{0,B} - \Delta\vec{V}_n\bar{Y}\cdot m_B} \tag{9}$$

Similarly, if the term $\Delta\vec{V}_n\hat{Y}$ is assumed negligible, then the same ratio can be obtained by (10).

$$\frac{\vec{I}_{F,A}}{\vec{I}_{F,B}} = \frac{\Delta\vec{I}_{2,A}}{\Delta\vec{I}_{2,B}} \tag{10}$$

Because $\hat{Y} \ll \bar{Y}$ in any real network, omitting $\Delta\vec{V}_n\hat{Y}$ in (10) is assumed to be a valid simplification. The term $\Delta\vec{V}_n\bar{Y}$ can however not be omitted from (9). It is shown in Section 5 that the contribution from the term $\Delta\vec{V}_n\hat{Y}$ is quite small in the test network considered in this paper, where the theoretical value of this component is approximately $0.9A$. For comparison, the term $\Delta\vec{V}_n\bar{Y}$ has a theoretical value of $168A$ in the same network.

Both of the above approaches for estimating the ratio of the fault current components can then be combined with (7). However, a note on the correct impedances should be considered first. So far, the mutual coupling between the phases has been neglected. When the mutual coupling is assumed to be zero, no difference exists between the per phase series reactance, positive sequence reactance or zero sequence reactance of the line. However, as the mutual coupling will be present in any real network, along with an earth return affecting the zero sequence currents, the fault current component ratio as expressed by (9) and (10) will not equal the ratio of the per phase series impedances. Instead, when combining (7) with either (9) or (10), the corresponding sequence impedance must be applied. Eqs. (11) and (12) illustrate this, where the subscripts "0" and "2" have been added to signify zero sequence and negative (and positive) sequence impedances, respectively.

$$\frac{|Z_{0,BF}|}{|Z_{0,AF}|} = \frac{|\Delta 3\vec{I}_{0,A} - \Delta\vec{V}_n\bar{Y}\cdot m_A|}{|\Delta 3\vec{I}_{0,B} - \Delta\vec{V}_n\bar{Y}\cdot m_B|} \tag{11}$$

$$\frac{|Z_{2,BF}|}{|Z_{2,AF}|} = \frac{|\Delta\vec{I}_{2,A}|}{|\Delta\vec{I}_{2,B}|} \tag{12}$$

In the following discussion, (11) is defined as the zero sequence method, and (12) as the negative sequence method.

3.2. Estimating m_A and m_B

As the term $\Delta\vec{V}_n\bar{Y}$ is significant, values for m_A, m_B and $\bar{Y}$ must be available in order for the zero sequence method to be applied. The factors m_A and m_B represent the division of the part of the zero sequence current which is driven by the neutral voltage, and they depend on the topology and line parameters of the ring-connected feeders and their laterals. In this paper, three methods for determining m_A and m_B are considered.

3.2.1. From line parameters

The ring is divided into n zero-sequence PI-equivalents, chosen so that the magnitude of the zero-sequence series impedance for each PI-section is the same, i.e. $|z_1| = |z_2| = |z_3| = \cdots = |z_n|$. The total capacitance of PI-section k is labelled C_k. Next, the parallel capacitances of adjacent PI-equivalents are summed, and $n+1$ capacitances $\tilde{C}_0 - \tilde{C}_n$ are defined in (13).

$$\tilde{C}_i = \begin{cases} \frac{C_i}{2} & x = 0, n \\ \frac{\tilde{C}_{i-1}+C_i}{2} & x = 1, 2, \ldots, n-1 \end{cases} \tag{13}$$

By assuming that all these capacitances experience the same voltage, V_0, and by applying the principle of current division, the expressions below for m_A and m_B can be derived:

$$m_A = \frac{\sum_{i=0}^{n}\tilde{C}_i\frac{n-i}{n}}{\sum_{i=0}^{n}\tilde{C}_i} \tag{14}$$

$$m_B = \frac{\sum_{i=0}^{n}\tilde{C}_i\frac{i}{n}}{\sum_{i=0}^{n}\tilde{C}_i} \tag{15}$$

Laterals on the feeders are simply accounted for by summing their entire zero-sequence capacitance to the corresponding $\tilde{C}_i$.

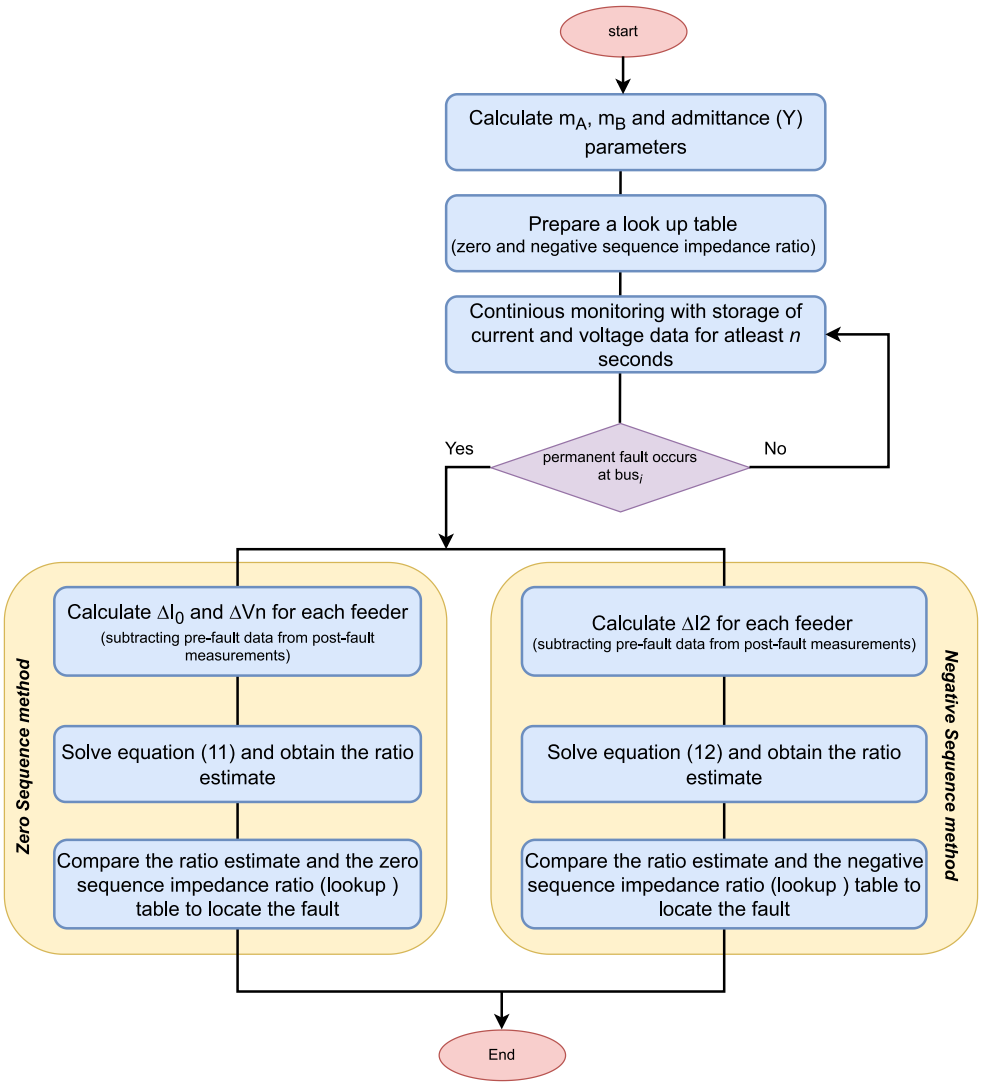

Fig. 5. The proposed earth fault location method.

3.2.2. Ratio of zero sequence currents

This approach is based on cases, either from fault records or earth fault tests, where an earth fault occurred either in the background network or at the substation. In such cases the fault current will not flow through the feeders forming the ring and the change in zero sequence current in these feeders will be due to the change in neutral voltage. Looking at (8), $\vec{I}_{F,A}$ and $\vec{I}_{F,B}$ will both be zero and hence the fraction of zero sequence current flowing through each feeders due to $\Delta\vec{V}_n$ can be obtained as described by (16).

$$\frac{\Delta\vec{I}_{0,A}}{\Delta\vec{I}_{0,B}} = \frac{m_A}{1-m_A} \tag{16}$$

By recognising that the factors m_A and m_B are real numbers, (16) can be further developed to produce (17).

$$m_A = \frac{|\,\Delta\vec{I}_{0,A}\,|}{|\,\Delta\vec{I}_{0,A}\,| + |\,\Delta\vec{I}_{0,B}\,|} \tag{17}$$

3.2.3. Ratio of zero sequence current and voltage

This approach considers a fault somewhere in the background network, at the main busbar, or at the beginning of one of the two feeders. For faults in the background network or at the main busbar $\vec{I}_{F,A}$ and $\vec{I}_{F,B}$ will be zero as established previously. If a fault occurs at the beginning of one of the feeders, the fault current component on the other feeder will be zero. Assume for instance that the fault occurred on the beginning of feeder B. If the neutral voltage is available in the fault records, the factor m_A can be obtained as described by (18).

$$m_A = \frac{|\Delta 3\vec{I}_{0,A}|}{|\Delta\vec{V}_n\bar{Y}|} \tag{18}$$

If the admittance $\bar{Y}$ is not known, or if it cannot be determined with sufficient accuracy, earth fault tests can be performed to obtain it along with m_A and m_B. By applying faults consecutively at the beginning of each feeder, the factors $\bar{Y}\cdot m_A$ and $\bar{Y}\cdot m_B$ can be obtained directly.

The flowchart of the proposed algorithm is shown in Fig. 5. Overall, the method requires to define system level parameters (such as m_A, m_B, $\bar{Y}$) beforehand and to store the pre-fault current and voltage measurements at the primary substation. When a fault occurs, Eqs. (11) and (12) are used to estimate ratio of fault currents in the two feeders forming the ring. The ratio estimate is then compared with the ideal impedance ratio and interpolation will be used to locate the earth fault.

4. System description and modelling

The test case network used for the evaluating the methods is based on an existing 22 kV distribution network. Network data have been provided by Norwegian network operator Elvia, and some changes have

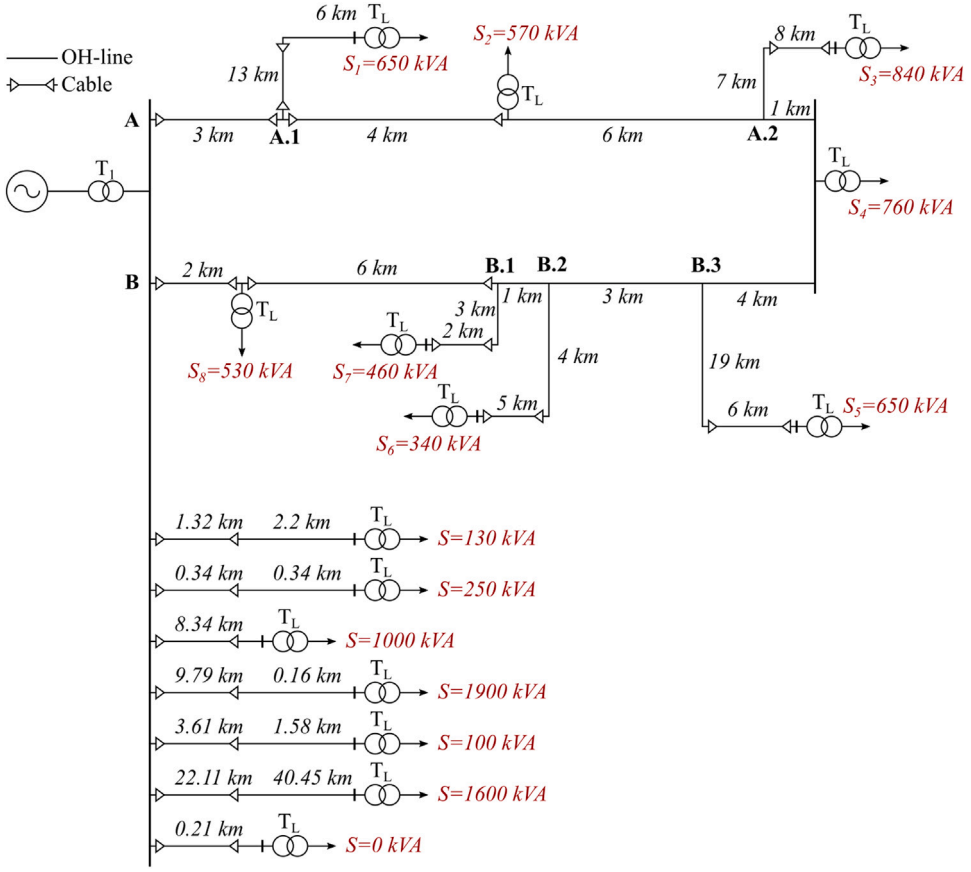

Fig. 6. Topology of ring-connected feeders A and B.

been made to the topology both to obtain the desired properties and to be able to disclose the model used.

The network consists of a single main transformer with isolated neutral supplying nine feeders connected at a main bus bar. The supplying grid is modelled as an ideal 132 kV voltage source with a source impedance modelled according IEC 60909 [43] to produce the desired short circuit capacity in the network. The short circuit power is expected to be in the range of 130–450 MVA, and the results are obtained using a 250 MVA source unless otherwise specified.

Feeders A and B have been connected to form a ring, and all faults are applied to these feeders. Fig. 6 shows the details of the ring connected feeders. Feeder A and B are modelled in greater detail, with five laterals included (A.1, A.2, B.1, B.2 and B.3), and with loads distributed around the ring. Furthermore, feeders A and B are modelled as series connected PI-segments of length 1 km to better represent the distributed nature of the line parameters. All the loads in the network are constant impedance loads with power factor 0.9 connected via load transformers. As a simplification, the other seven feeders C-I are modelled without laterals and with loads concentrated at the feeder ends. Complete network data can be found in Table 1.

Table 1
Test network and model parameters.

Network data	
OH-line	3-phase PI-section: 50 Hz, R=0.077 Ω/km, X=0.34 Ω/km, C=10.806 nF/km, R_0 = 0.413 Ω/km, X_0 = 1.134 Ω/km, C_0=5.976 nF/km, G_0=37.55 nS/km. Asymmetry: 2% and 3% are added to C_0 in phases *a* and *b*, respectively.
Cable	3-phase PI-section: 50 Hz, R=0.125 Ω/km, X=0.11 Ω/km, C = C_0=0.28 μF/km. Asymmetry: 1% and 2% are added to C_0 in phases *a* and *c*, respectively.
Main transformer	100 MVA 132/22 kV Dy1 transformer. X=6%, R=0.25%. Modelled using the Hybrid transformer model in ATPDraw with typical values for inductance and resistance, no capacitance or core effects included.
Load transformers	2 MVA 22/0.4 kV Dy1 transformer grounded on the LV-side. X=5%, R=0.78%. Modelled using the Hybrid transformer model in ATPDraw with typical values for inductance and resistance, no capacitance or core effects included.
Loads	Grounded Y-connected constant impedance loads.
Simulation and data processing	
Sample rate: 2 kHz. Matlab-designed equiripple FIR high-pass filter: f_{pass} = 45 Hz, passband ripple = 0.1 dB. Software: ATPDraw version 7.2p11.	

5. Simulation result and analysis

The methods are tested for earth faults at 30 different fault locations evenly spaced around the ring, i.e. every km. The distance to fault is measured from the beginning of feeder A for all cases. The parameters m_A and m_B are set to m_A = 0.5486 and m_B = 0.4514, obtained by applying a fault at the main bus bar and using (17). For comparison, the estimation of m_A and m_B from line parameters yielded m_A = 0.5489 and m_B = 0.4511.

The final estimates produced by each method are obtained as the average estimates between 250 ms and 270 ms after fault inception to allow for steady state conditions, whereas the pre-fault values are obtained 150 ms before fault inception.

5.1. Fault resistance and load asymmetry

Both the fault resistance and the load symmetry is varied. The load symmetry is varied by changing the load impedance in the individual

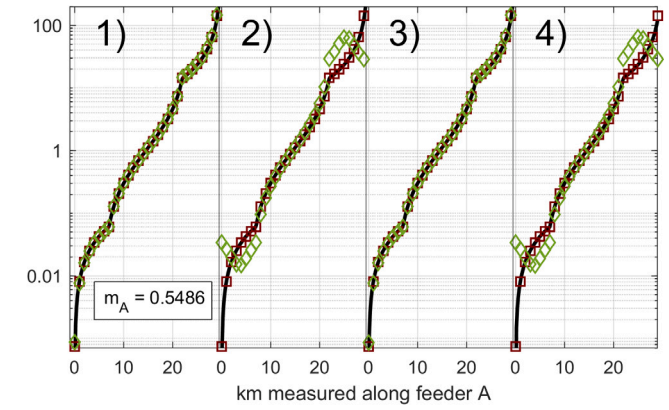

(a) Zero sequence method

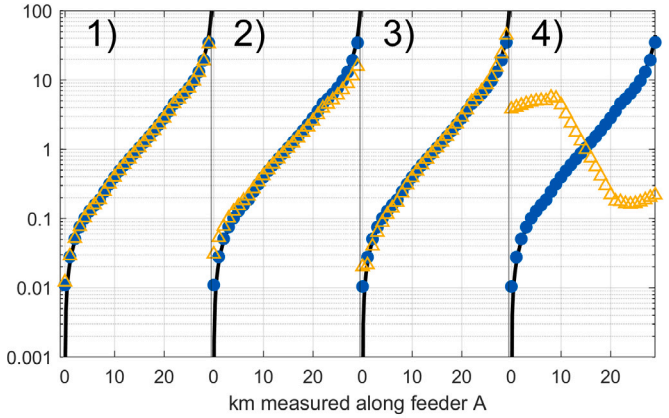

(b) Negative sequence method

Fig. 7. Results for scenarios 1–4. Simplified versions not considering pre-fault values are included for reference.

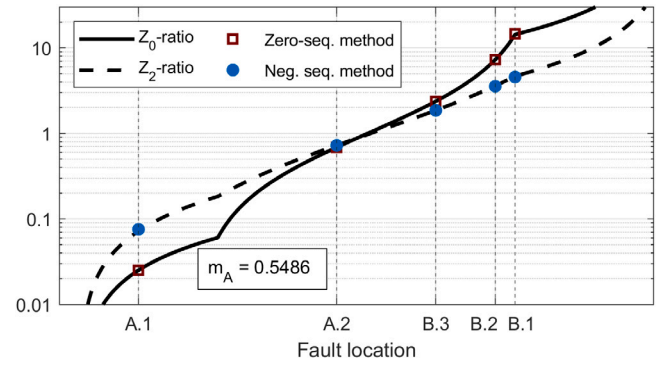

Fig. 8. Zero sequence method and negative sequence method results when faults occur on laterals.

phases of the load supplied by the ring, whereas the other loads in the system remain balanced. During asymmetrical loading, the load impedance of phases a, b, and c are Z_L, $1.1{\cdot}Z_L$ and $0.9{\cdot}Z_L$, respectively, where Z_L is the per phase impedance corresponding to the nominal loads S1-S8 in Fig. 6. The following four scenarios are then considered:

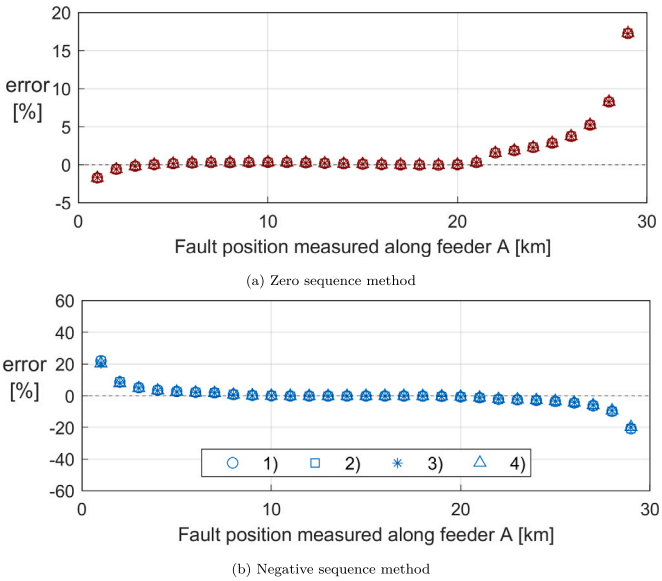

(a) Zero sequence method

(b) Negative sequence method

Fig. 9. Percentage errors for both methods in scenario 1–4.

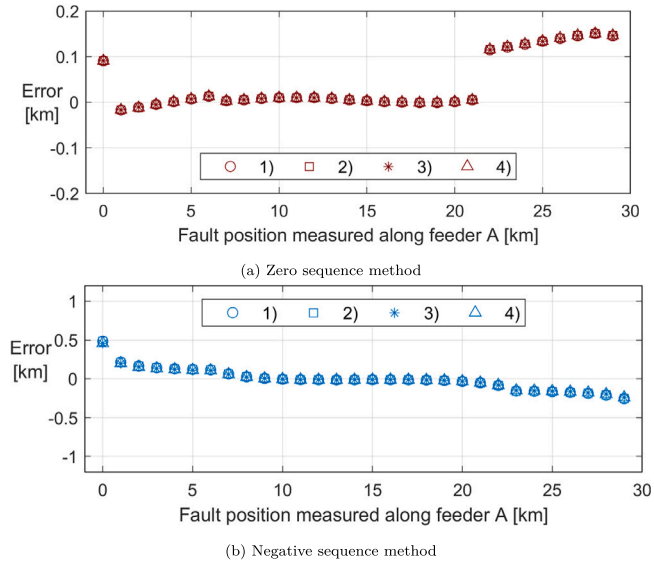

(a) Zero sequence method

(b) Negative sequence method

Fig. 10. Distance estimate errors for both methods in scenario 1–4.

1. $R_f = 1\ \Omega$, symmetrical load
2. $R_f = 1\ \text{k}\Omega$, symmetrical load
3. $R_f = 1\ \Omega$, asymmetrical load
4. $R_f = 1\ \text{k}\Omega$, asymmetrical load

The results are shown in Fig. 7. The results show that both methods are resilient against load asymmetry and fault resistance. Fig. 7(a) shows that applying the zero sequence method without considering pre-fault values can provide reasonable accuracy for low impedance faults, whereas the accuracy is drastically reduced for large fault resistances. The zero sequence method is however unaffected by the load asymmetry, even when pre-fault values are not considered. Fig. 7(b) illustrates that the application of negative sequence currents directly without subtracting their pre-fault values, as done in [44], is only a viable option for low impedance faults. Unbalanced loads also have a negative impact on this particular method, especially in conjunction with a large fault resistance.

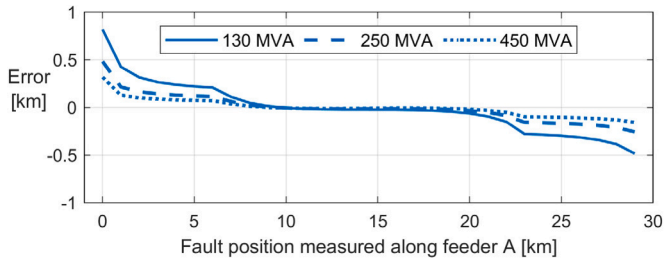

Fig. 11. Distance estimate errors for negative sequence method for different source impedances.

To investigate the effect of faults on laterals, faults are applied to each of the five laterals in turn. The faults are applied at the intersection of the cable and OH-lines on the laterals, and the results are shown in Fig. 8. Both methods see these faults as if they occurred at the connection point between the lateral and the ring itself. No variation was observed across scenarios 1–4 in these fault cases.

Fig. 9 shows the percentage prediction error for the two methods in the four scenarios considered above, where positive errors correspond overestimating the impedance ratio. Fig. 10 shows the errors in absolute distance. It can be seen that when mapped to this view, the seemingly large errors towards the line ends are less pronounced. As the slope of the impedance ratio is quite steep towards the ends, an error in the estimate ratio translates to a relatively small error in distance estimate compared to faults in the middle of the ring. This presentation also shows the discontinuities in the graph more clearly, which occur due to the different impedances of the cable sections and the OH-lines.

Figs. 9 and 10 suggest that the methods are complementary, and that their simultaneous application may yield better results. In the scenarios shown in the figures this would be the case, but as shown later in the paper, the two methods will not be complementary in the presence of measurement errors and other imperfections. Therefore, an average of the two methods is not guaranteed to give any real improvements.

The figures confirm that the zero sequence method and the negative sequence method have pretty similar performance in all the four scenarios. Both methods show good accuracy for faults in the middle of the line, whereas the accuracy tapers off towards the outer ends of the ring. For the negative sequence method this is in part assumed to be caused by the terms $\Delta\vec{V}_n\hat{Y}\cdot q_A$ and $\Delta\vec{V}_n\hat{Y}\cdot q_B$ in (8), which were assumed negligible when deriving (12). As the fault is moved closer to either end of the ring, for instance at the beginning of feeder A, the fault current component on feeder B should in theory approach 0. The terms $\Delta\vec{V}_n\hat{Y}\cdot q_A$ and $\Delta\vec{V}_n\hat{Y}\cdot q_B$ are then no longer negligible. For instance, assuming that $\Delta\vec{V}_n \approx \frac{22}{\sqrt{(3)}}kV$, the term $\Delta\vec{V}_n\hat{Y}$ should be approximately $0.9A$, which is close to the observed value of $\Delta\vec{I}_{2,B} = 1.2A$ when the fault occurs close to terminal A. A similar argument can be made to explain why the zero sequence method shows poorer accuracy near the two ends of the ring, although this method is sensitive to a variety of parameters as will be discussed in later sections of this paper.

The main source of error for the negative sequence method is however the source impedance of the network. If this is assumed to be very large, the negative sequence method becomes less accurate. Fig. 11 illustrates to impact of the source impedance as the short circuit capacity is varied between 130 MVA and 450 MVA. When the short circuit capacity increases and the source impedance decreases, the estimation error is reduced. However, even with a stiff grid the error does not reach zero, suggesting that the factors discussed above are of some importance. The zero sequence method is not affected by this parameter.

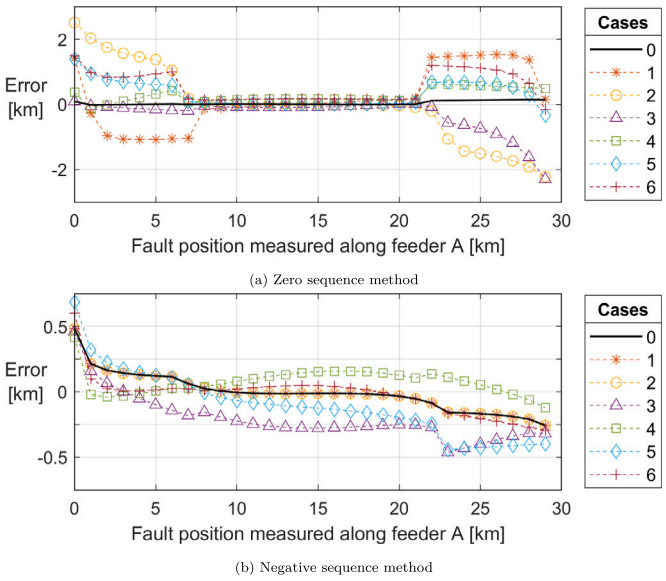

(a) Zero sequence method

(b) Negative sequence method

Fig. 12. Distance estimate errors for both methods considering current measurement errors.

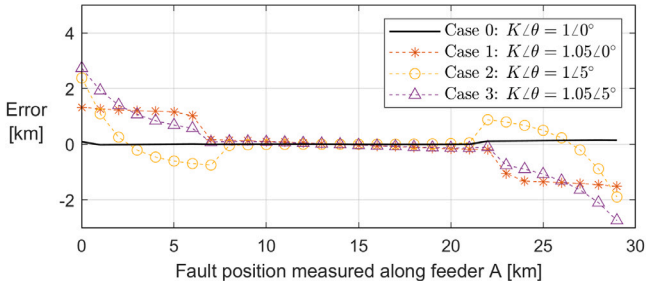

Fig. 13. Zero sequence method distance estimate error for various neutral voltage measurement errors.

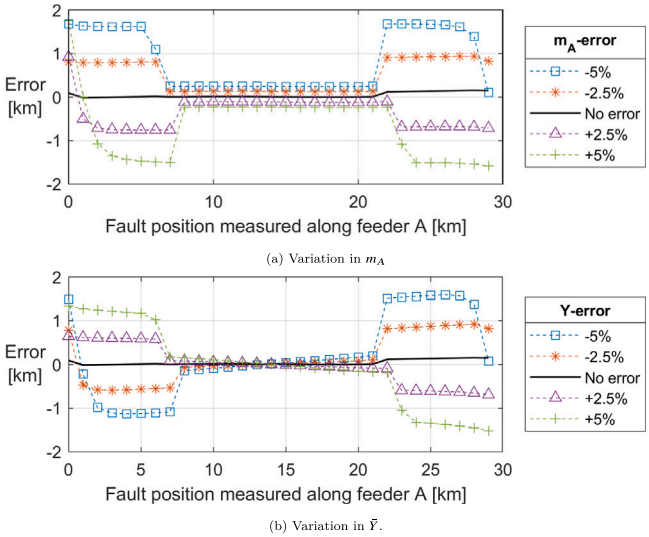

(a) Variation in m_A

(b) Variation in $\bar{Y}$.

Fig. 14. Zero sequence method distance estimate error for inaccurate values of m_A and $\bar{Y}$.

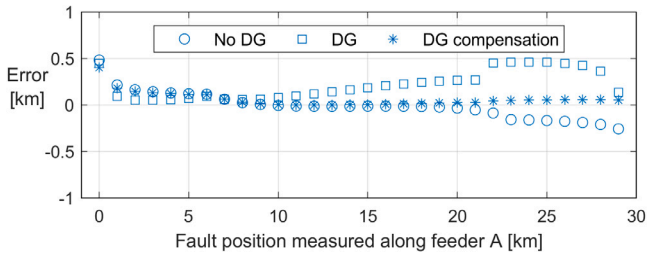

Fig. 15. Impact of DG on the negative sequence method.

Table 2
Phase current measurement errors.

Case	$K\angle\theta$					
	Feeder B			Feeder A		
	Ph. a	Ph. b	Ph. c	Ph. a	Ph. b	Ph. c
0	$1\angle0°$	$1\angle0°$	$1\angle0°$	$1\angle0°$	$1\angle0°$	$1\angle0°$
1	$1.05\angle0°$	$1.05\angle0°$	$1.05\angle0°$	$1.05\angle0°$	$1.05\angle0°$	$1.05\angle0°$
2	$1\angle5°$	$1\angle5°$	$1\angle5°$	$1\angle5°$	$1\angle5°$	$1\angle5°$
3	$1\angle0°$	$1\angle0°$	$1\angle0°$	$1.05\angle5°$	$1.05\angle5°$	$1.05\angle5°$
4	$1.5\angle0°$	$1.02\angle0°$	$0.96\angle0°$	$1.01\angle0°$	$1.03\angle0°$	$0.99\angle0°$
5	$1\angle5°$	$1\angle2°$	$1\angle1°$	$1\angle-5°$	$1\angle-4°$	$1\angle2°$
6	$1.05\angle5°$	$1.02\angle2°$	$0.96\angle1°$	$1.01\angle-5°$	$1.03\angle-4°$	$0.99\angle2°$

Overall, the simulation analysis showed that the negative sequence method can locate earth faults with a ±250-meter margin for most fault locations around the ring, and in the worst case, there is a ±500-meter error margin for fault locations close to the end of the lines. The negative sequence method is unaffected by variations in fault resistance and load symmetry. The short circuit capacity of the network does however impact the results. The zero sequence method can locate earth faults within a ±150-meter margin for most fault locations, and is not affected by fault resistance, load symmetry or the short circuit capacity of the network.

5.2. Measurement errors

The performance of the two methods were investigated against measurement inaccuracies. To emulate measurement errors, the measured phasors are multiplied by some disturbance $K\angle\theta$.

5.2.1. Phase currents

Measurement errors are applied to each of the six phase currents measured on feeders A and B, as described by Table 2. Scenario (1) is considered, and the distance error for both methods with the various combinations of measurement errors applied are showed in Figs. 12(a) and 12(b).

The results show that symmetrical measurement errors, i.e. the same measurement error in all the six current transformers (CTs), have no visible effect on the negative sequence results, whereas the zero sequence method is affected. This is as expected when inspecting (12), in which symmetrical measurement errors applied to the negative sequence measurements will cancel. Eq. (11) shows that this is not the case for the zero sequence method, as the nominator and denominator will not be equally affected.

The unsymmetrical measurement errors will as expected have a negative effect on both methods, although it is less apparent how a particular set of measurement errors will affect the accuracy at various fault locations. It is noted that symmetrical measurement errors within each set of measurements at terminal A and B, here represented by case 3, still gives a considerable negative effect on the results.

The measurement errors also accentuates the effect of the different line segments. Faults occurring in the overhead line consistently produces lower distance estimate errors in the case of the zero sequence methods, whereas the negative sequence method generally becomes less accurate for faults in the overhead line. However, the magnitude of the errors are significantly larger for the zero sequence method, whereas the negative sequence method accuracy is mostly kept within $\pm500m$.

In a realistic implementation the zero sequence method could however utilise zero sequence current transformers to measure the zero sequence current directly, and thus achieve higher measurement accuracy than the phase current measurements.

5.2.2. Neutral voltage

Measurement errors are applied to the neutral voltage measurements in the same way as was done for the phase currents, and both the cases and the results are shown in Fig. 13. Compared to the effect of phase current measurement errors, the measurement error in neutral voltage gives a similar reduction in precision for the zero sequence method, with a reduced precision towards the ends of the ring. The negative sequence method is obviously not impacted by this measurement.

5.3. Other sensitivity analysis

The zero sequence method requires values for the ring admittance to ground $\bar{Y}$, as well as m_A and m_B. These values are varied within ±5% of their correct values, and the resulting errors are shown in Fig. 14. Note that the parameter $\bar{Y}$ also includes the admittance to ground of the laterals connected to feeders A and B, not just the admittances of A and B.

Both variation in m-values and $\bar{Y}$ result in a significant degradation of the zero sequence method results. Variation in m_A has a greater impact on the results than variation in $\bar{Y}$, as is expected when considering (11). As $m_B = 1 - m_A$, variation in m_A is necessarily accompanied by variation in m_B, which gives a larger impact than simply varying $\bar{Y}$.

Eq. (11) also has the interesting property of becoming independent of $\bar{Y}$ at the fault location corresponding to

$$\frac{Z_{0,BF}}{Z_{0,AF}} = \frac{m_A}{m_B}$$

This effect is observed at approximately 13 km, where the zero sequence method produce the same result regardless of $\bar{Y}$.

The methods have also been tested in a compensated network, as well as a network without any background network, both of which yielded good results. A reduction in accuracy was however observed, particularly for the compensated network, suggesting that the fault current level will have an impact on the methods.

The behaviour of the two methods during two phase and three phase short circuit faults was investigated briefly. The negative sequence method works for two-phase short circuits as well as some three-phase faults, though it appears dependent on the short circuit capacity of the network. The zero sequence method is only valid for single phase faults.

During testing of the methods it was observed that the zero sequence method was much more sensitive to large fault resistances when unfiltered measurements were used. This occurred due to the slow exponential decay which is observed in the neutral voltage and the fault current for high impedance faults. Although this effect was also observed for the negative sequence method, the effect on the distance estimates was much less pronounced. Including a high-pass filter therefore becomes critical when applying the zero sequence method.

Lastly, the presence of DG in the network was investigated briefly. A source rated at approximately 1 MVA was added to the network in parallel with load S_2, and scenario (1) from earlier was evaluated with and without the presence of this DG. As expected, the presence of the generator had a minor impact on the negative sequence method as shown in Fig. 15. If the negative sequence current is measured at the DG location, the effect of the DG can however be eliminated. The negative sequence current measured at the DG will be observable in the measurements at feeders A and B, and the magnitude of this current

in these two locations can simply be estimated using current division between the DG location and the main bus. The DG current can then be eliminated from the measurements on feeders A and B, and the result of compensating for the effect of the DG in this way is also shown in Fig. 15. Using such an approach will however turn the method into a wide-area method with added complexity, and given the small impact of the DG on the results this may not be necessary. Finally, as the DG is separated from the network via a load transformer, the zero sequence method is not impacted by DG in the network.

6. Conclusion

This paper has presented two novel methods for locating earth faults in a MV distribution network. The two methods are based on utilising the ratio of change in zero and negative sequence current during fault on ring-connected feeders, though one of the methods also requires zero sequence voltage measurements. Compared to previous work, the paper have made the following contributions: (1) improved accuracy of earth fault location compared to methods not considering pre-fault measurement; (2) provided equations describing sequence currents in a ring network, particularly the division of zero sequence currents among two ring-connected feeders. The paper also provides experimental approaches for determining this division of zero sequence currents.

The two methods developed in this paper show good accuracy in fault location. The negative sequence method yielded maximum distance estimate errors in the range of 0.3–1 km in the test network, depending measurement errors and on the assumed source impedance of the supplying network. The zero sequence method yielded errors less than 200 m in the ideal cases, but the estimation error increased when measurement errors were applied. Fault resistance and unbalanced loads have little effect on either of the methods, whereas inaccurate current and voltage measurements represent the largest sources of error. The negative sequence method appears to be robust against most sources of error. The measurement of negative sequence currents may however not be readily available in most distribution networks, and the method is affected by the source impedance of the supplying network. The zero sequence method is likely easier to implement due to the availability of measurements, but it is relatively less robust due to its dependency on several uncertain parameters.

The size of the background network have been found to have little effect on the method, although this has not been tested extensively. The methods have also been verified in a resonance grounded system where it yielded promising results, though further testing is required in order to describe the performance properly in such networks.

Future work will mainly focus on further testing of the methods on a laboratory setup and later on a real power grid network.

CRediT authorship contribution statement

Tesfaye Amare Zerihun: Conceptualization, Methodology, Software, Validation, Formal Analysis,Visualisation, Investigation, Writing – original draft, Writing – review & editing. **Thomas Treider:** Conceptualization, Methodology, Software, Validation , Formal Analysis,Visualisation, Investigation, Writing – original draft, Writing – review & editing. **Henning Taxt:** Conceptualization, Methodology, Writing – review & editing, Supervision. **Lars B. Nordevall:** Conceptualization, Writing – review & editing, Supervision. **Thomas S. Haugan:** Methodology, Software, Writing – review & editing.

Declaration of competing interest

The authors declare that they have no known competing financial interests or personal relationships that could have appeared to influence the work reported in this paper.

Acknowledgements

This paper has been funded by the CINELDI - Centre for intelligent electricity distribution, an 8 year Research Centre under the Research Council of Norway's FME-scheme (Centre for Environment-friendly Energy Research, 257626/E20), and the Norwegian Research Council project ProDig (295034/E20). The authors gratefully acknowledge the financial support from the Research Council of Norway and the CINELDI and ProDig partners.

References

[1] S. Hänninen, et al., Single Phase Earth Faults in High Impedance Grounded Networks: Characteristics, Indication and Location, VTT Technical Research Centre of Finland, 2001.

[2] F. Aboshady, D. Thomas, M. Sumner, A new single end wideband impedance based fault location scheme for distribution systems, Electr. Power Syst. Res. 173 (2019) 263–270.

[3] R. Dashti, J. Sadeh, Accuracy improvement of impedance-based fault location method for power distribution network using distributed-parameter line model, Int. Trans. Electr. Energy Syst. 24 (3) (2014) 318–334.

[4] R. Dashti, J. Sadeh, Applying dynamic load estimation and distributed-parameter line model to enhance the accuracy of impedance-based fault-location methods for power distribution networks, Electr. Power Compon. Syst. 41 (14) (2013) 1334–1362.

[5] A.D. Filomena, M. Resener, R.H. Salim, A.S. Bretas, Fault location for underground distribution feeders: An extended impedance-based formulation with capacitive current compensation, Int. J. Electr. Power Energy Syst. 31 (9) (2009) 489–496, http://dx.doi.org/10.1016/j.ijepes.2009.03.026, URL https://www.sciencedirect.com/science/article/pii/S0142061509000544, Power Systems Computation Conference (PSCC) 2008.

[6] Y. Liao, Generalized fault-location methods for overhead electric distribution systems, IEEE Trans. Power Deliv. 26 (1) (2011) 53–64, http://dx.doi.org/10.1109/TPWRD.2010.2057454.

[7] A. Nikander, P. Jarventausta, Methods for earth fault identification and distance estimation in a compensated medium voltage distribution network, in: Proceedings of EMPD '98. 1998 International Conference on Energy Management and Power Delivery, Vol. 2, Cat. No.98EX137, 1998, pp. 595–600 vol.2, http://dx.doi.org/10.1109/EMPD.1998.702754.

[8] M.A. Aftab, S.S. Hussain, I. Ali, T.S. Ustun, Dynamic protection of power systems with high penetration of renewables: A review of the traveling wave based fault location techniques, Int. J. Electr. Power Energy Syst. 114 (2020) 105410, http://dx.doi.org/10.1016/j.ijepes.2019.105410, URL https://www.sciencedirect.com/science/article/pii/S0142061518331594.

[9] C.Y. Evrenosoglu, A. Abur, Fault location in distribution systems with distributed generation, in: Proc. Power Systems Computation Conference, 2005.

[10] D. Coggins, D.W. Thomas, B.R. Hayes-Gill, Y. Zhu, An fpga based travelling-wave fault location system, in: 2007 International Conference on Field-Programmable Technology, IEEE, 2007, pp. 277–280.

[11] H. Liu, X. Zeng, Y. Wang, F. Peng, Research on travelling wave transmission characteristics in distribution network, in: 2012 China International Conference on Electricity Distribution, IEEE, 2012, pp. 1–5.

[12] A. Farughian, L. Kumpulainen, K. Kauhaniemi, Review of methodologies for earth fault indication and location in compensated and unearthed MV distribution networks, Electr. Power Syst. Res. 154 (2018) 373–380.

[13] R. Dashti, M. Tahavori, M. Daisy, H.R. Shaker, A new matching algorithm for fault section estimation in power distribution networks, in: 2018 International Symposium on Advanced Electrical and Communication Technologies, ISAECT, IEEE, 2018, pp. 1–4.

[14] E. Gord, R. Dashti, M. Najafi, H.R. Shaker, Real fault section estimation in electrical distribution networks based on the fault frequency component analysis, Energies 12 (6) (2019) 1145.

[15] J. Mora-Florez, V. Barrera-Nunez, G. Carrillo-Caicedo, Fault location in power distribution systems using a learning algorithm for multivariable data analysis, IEEE Trans. Power Deliv. 22 (3) (2007) 1715–1721, http://dx.doi.org/10.1109/TPWRD.2006.883021.

[16] F. Chunju, K. Li, W. Chan, Y. Weiyong, Z. Zhaoning, Application of wavelet fuzzy neural network in locating single line to ground fault (SLG) in distribution lines, Int. J. Electr. Power Energy Syst. 29 (6) (2007) 497–503, http://dx.doi.org/10.1016/j.ijepes.2006.11.009, URL https://www.sciencedirect.com/science/article/pii/S0142061506002092.

[17] M. Pourahmadi-Nakhli, A.A. Safavi, Path characteristic frequency-based fault locating in radial distribution systems using wavelets and neural networks, IEEE Trans. Power Deliv. 26 (2) (2010) 772–781.

[18] X. Deng, R. Yuan, Z. Xiao, T. Li, K.L.L. Wang, Fault location in loop distribution network using SVM technology, Int. J. Electr. Power Energy Syst. 65 (2015) 254–261, http://dx.doi.org/10.1016/j.ijepes.2014.10.010, URL https://www.sciencedirect.com/science/article/pii/S0142061514006139.

[19] G. Liang, P. Liyuan, L. Ruihuan, Z. Fen, W. Xin, Fault location in distribution network with distributed generation based on neural network, in: 2014 China International Conference on Electricity Distribution, CICED, IEEE, 2014, pp. 209–212.
[20] A.C. Adewole, R. Tzoneva, S. Behardien, Distribution network fault section identification and fault location using wavelet entropy and neural networks, Appl. Soft Comput. 46 (2016) 296–306.
[21] K. Jia, Z. Ren, T. Bi, Q. Yang, Ground fault location using the low-voltage-side recorded data in distribution systems, IEEE Trans. Ind. Appl. 51 (6) (2015) 4994–5001, http://dx.doi.org/10.1109/TIA.2015.2425358.
[22] F.C.L. Trindade, W. Freitas, J.C.M. Vieira, Fault location in distribution systems based on smart feeder meters, IEEE Trans. Power Deliv. 29 (1) (2014) 251–260, http://dx.doi.org/10.1109/TPWRD.2013.2272057.
[23] J. Altonen, A. Wahlroos, Performance of modern fault passage indicator concept in compensated MV-networks, in: CIRED Workshop 2016, IET, 2016, pp. 1–4.
[24] J.-H. Teng, W.-H. Huang, S.-W. Luan, Automatic and fast faulted line-section location method for distribution systems based on fault indicators, IEEE Trans. Power Syst. 29 (4) (2014) 1653–1662.
[25] R. Calone, A. Cerretti, A. Fatica, Evolution of the fault locator on MV distribution networks: From simple stand alone device, to a sophisticated strategic component of the smart grid control system, in: Proc. 21st Int. Conf. Exhib. Electr. Distrib., CIRED, 2011.
[26] M. Pignati, L. Zanni, P. Romano, R. Cherkaoui, M. Paolone, Fault detection and faulted line identification in active distribution networks using synchrophasors-based real-time state estimation, IEEE Trans. Power Deliv. 32 (1) (2016) 381–392.
[27] S. Jamali, A. Bahmanyar, E. Bompard, Fault location method for distribution networks using smart meters, Measurement 102 (2017) 150–157, http://dx.doi.org/10.1016/j.measurement.2017.02.008, URL https://www.sciencedirect.com/science/article/pii/S0263224117301033.
[28] D. Topolanek, P. Toman, V. Jurak, M. Jurík, J. Jiricka, J. Drápela, Evaluation of the New Method Vdip for an Earth Fault Location, AIM, 2019.
[29] L.J. Awalin, H. Mokhlis, A.H.A. Halim, Improved fault location on distribution network based on multiple measurements of voltage sags pattern, in: 2012 IEEE International Conference on Power and Energy, PECon, 2012, pp. 767–772, http://dx.doi.org/10.1109/PECon.2012.6450319.
[30] M.A. Elsadd, N.I. Elkalashy, T.A. Kawady, A.-M.I. Taalab, M. Lehtonen, Incorporating earth fault location in management-control scheme for distribution networks, IET Gener. Transm. Distrib. 10 (10) (2016) 2389–2398.
[31] P. Bountouris, H. Guo, D. Tzelepis, I. Abdulhadi, F. Coffele, C. Booth, MV faulted section location in distribution systems based on unsynchronized LV measurements, Int. J. Electr. Power Energy Syst. 119 (2020) 105882.
[32] D. Topolanek, M. Lehtonen, P. Toman, J. Orsagova, J. Drapela, An earth fault location method based on negative sequence voltage changes at low voltage side of distribution transformers, Int. J. Electr. Power Energy Syst. 118 (2020) 105768.
[33] A. Farughian, L. Kumpulainen, K. Kauhaniemi, Earth fault location using negative sequence currents, Energies 12 (19) (2019) 3759.
[34] M. Lehtonen, O. Siirto, M.F. Abdel-Fattah, Simple fault path indication techniques for earth faults, in: 2014 Electric Power Quality and Supply Reliability Conference, PQ, IEEE, 2014, pp. 371–378.
[35] A. Silos-Sanchez, R. Villafafila-Robles, P. Lloret-Gallego, Novel fault location algorithm for meshed distribution networks with DERs, Electr. Power Syst. Res. 181 (2020) 106182.
[36] K. Sun, Q. Chen, P. Zhao, Automatic faulted feeder section location and isolation method for power distribution systems considering the change of topology, Energies 10 (8) (2017) 1081.
[37] A. Mohamed, B. Younes, T. Lamhamdi, H. El Moussaoui, H. El Markhi, Fault location and isolation technique in smart distribution systems with distributed generation, in: 2020 1st International Conference on Innovative Research in Applied Science, Engineering and Technology, IRASET, IEEE, 2020, pp. 1–5.
[38] M.A. Ataei, M. Gitizadeh, M. Lehtonen, R. Razavi-Far, Multi-agent based protection scheme using current-only directional overcurrent relays for looped/meshed distribution systems, IET Gener. Transm. Distrib. 16 (8) (2022) 1567–1581.
[39] T. Zhang, H. Yu, P. Zeng, L. Sun, C. Song, J. Liu, Single phase fault diagnosis and location in active distribution network using synchronized voltage measurement, Int. J. Electr. Power Energy Syst. 117 (2020) 105572, http://dx.doi.org/10.1016/j.ijepes.2019.105572, URL https://www.sciencedirect.com/science/article/pii/S0142061519314887.
[40] H. Saadat, Power System Analysis, third ed., PSA Publishing, S.l., 2010.
[41] M. Loos, S. Werben, J.C. Maun, Circulating currents in closed loop structure, a new problematic in distribution networks, in: 2012 IEEE Power and Energy Society General Meeting, 2012, pp. 1–7, http://dx.doi.org/10.1109/PESGM.2012.6344889.
[42] A. Kalyuzhny, G. Kushnir, Analysis of current unbalance in transmission systems with short lines, IEEE Trans. Power Deliv. 22 (2) (2007) 1040–1048, http://dx.doi.org/10.1109/TPWRD.2006.883011.
[43] Short-circuit currents in three-phase A.C. systems - Part 0: Calculation of currents, 2016.
[44] M. Biller, J. Jaeger, Novel distance protection algorithm based on current comparison for closed-ring structures with distributed generation, in: 15th International Conference on Developments in Power System Protection, DPSP 2020, 2020, pp. 1–6, http://dx.doi.org/10.1049/cp.2020.0043.